Correlating contact line capillarity and dynamic contact angle hysteresis in surfactant-nanoparticle based complex fluids

A. R. Harikrishnan, Purbarun Dhar, Prabhat K. Agnihotri, Sateesh Gedupudi, and Sarit K. Das

Citation: Physics of Fluids **30**, 042006 (2018); doi: 10.1063/1.5020334
View online: https://doi.org/10.1063/1.5020334
View Table of Contents: http://aip.scitation.org/toc/phf/30/4
Published by the American Institute of Physics

Correlating contact line capillarity and dynamic contact angle hysteresis in surfactant-nanoparticle based complex fluids

A. R. Harikrishnan,[1,a)] Purbarun Dhar,[2,b)] Prabhat K. Agnihotri,[2] Sateesh Gedupudi,[1] and Sarit K. Das[1,c)]
[1]*Department of Mechanical Engineering, Indian Institute of Technology Madras, Chennai 600036, India*
[2]*Department of Mechanical Engineering, Indian Institute of Technology Ropar, Rupnagar 140001, India*

(Received 22 December 2017; accepted 26 March 2018; published online 11 April 2018)

Dynamic wettability and contact angle hysteresis can be correlated to shed insight onto any solid-liquid interaction. Complex fluids are capable of altering the expected hysteresis and dynamic wetting behavior due to interfacial interactions. We report the effect of capillary number on the dynamic advancing and receding contact angles of surfactant-based nanocolloidal solutions on hydrophilic, near hydrophobic, and superhydrophobic surfaces by performing forced wetting and de-wetting experiments by employing the embedded needle method. A segregated study is performed to infer the contributing effects of the constituents and effects of particle morphology. The static contact angle hysteresis is found to be a function of particle and surfactant concentrations and greatly depends on the nature of the morphology of the particles. An order of estimate of line energy and a dynamic flow parameter called spreading factor and the transient variations of these parameters are explored which sheds light on the dynamics of contact line movement and response to perturbation of three-phase contact. The Cox-Voinov-Tanner law was found to hold for hydrophilic and a weak dependency on superhydrophobic surfaces with capillary number, and even for the complex fluids, with a varying degree of dependency for different fluids. *Published by AIP Publishing.*
https://doi.org/10.1063/1.5020334

I. INTRODUCTION

Much of the recent research has been focused on the nanocolloidal suspensions, which are dispersions of nanoscale particles in base fluids, due to its promising applicability and utility in varied engineering domains.[1–3] Wettability is a principle phenomenon, which governs the performance of many engineering devices.[4] Control of wetting of liquid drops is of predominant importance in various technological applications, such as contact dispensing, inkjet printing, spray cooling, and in agrochemical applications.[5,6] However, the wetting angle or the equilibrium contact angle is not a true representation of the fluid-substrate interaction due to surface heterogeneity.[7] The information about the advancing contact angle (ACA) and the receding contact angle (RCA) gives a true representation of the resulting fluid-substrate interaction, and hence hysteresis is an important parameter influencing the performance of many engineering devices.

There is a large body of the literature which deals with the hysteresis and the relationship of hysteresis with the equilibrium contact angle.[8,9] Most of the studies are limited to normal fluids (mostly water) on surfaces of different hydrophobicities and surface textures.[10,11] Theoretical studies on dynamic contact angle hysteresis have been focused on mechanisms driving the contact line motion.[7] Accordingly, many theories have been developed such as hydrodynamic theory considering the viscous flow,[12,13] molecular kinetic theory considering the attachment or detachment of molecules near the contact line,[14] and a combined model incorporating the effects of the hydrodynamic model and kinetic model.[15] Studies focused mainly on probing the physics of contact angle hysteresis on nanocolloidal solutions on different substrates are rare.[16] However, in the recent past, there are tremendous studies devoted to the static contact angle measurement of nanocolloids on different substrates.[16–19] These studies have reported the effect of surface tension, roughness, and particle concentration on wetting angle and also tried to explore the physics governing the wetting. Also, the spreading dynamics of these nanocolloids and the forces driving the spreading have also been explored.[20,21] The present authors have tried to address the static hysteresis behavior in such nanocolloidal fluids on different surfaces in a recent study.[16] Lu *et al.* conclude from a list of recent studies on dynamic wetting characteristics that it is difficult to draw a general conclusion from the state of art of the literature as the nanocolloidal system is so complex because of the number phenomenon involved such Brownian dynamics, interfacial adsorption, deposition, and modification of topography of the substrate and layering of the particle near the three-phase contact line.[11] However, the study is limited to only a few cases and does not talk about the mechanisms and implications of the effect of particles and surfactants in modulating the hysteresis behavior on different substrates. Most of the studies on wetting characteristics off nanocolloids are limited to hydrophilic and hydrophobic substrates. However, the engineering community is presently focused on the superhydrophobic surfaces. Superhydrophobic surfaces are an

[a)]Electronic mail: harianilakkad@gmail.com
[b)]Electronic mail: purbarun@iitrpr.ac.in. Telephone: +91-1881-2173.
[c)]Electronic mail: skdas@iitrpr.ac.in. Telephone: +91-1881-24-2101.

integral part of the nature as we can observe in many plants and insects.[22–24] They are characterized by a large static advancing contact angle and a low hysteresis. They find applications in many engineering problems such as the self-cleaning surfaces, such as solar panels, lenses, and mirrors, area of reversible superhydrophobicity, and drag reduction in underwater applications.[25]

Kim *et al.*[26] reported the effect of capillary numbers or the velocity of the three-phase contact line on the dynamic advancing and receding contact angle on hydrophobic and superhydrophobic surfaces with a series of normal fluids using the Wilhelmy plate method. The dynamic receding contact angle response on superhydrophobic surfaces was found to decrease with increasing capillary number. However, the presence of slip on the superhydrophobic surface was found to result in a shift in the onset of dynamic contact angle variation with capillary number. To the best of authors' knowledge, there are no studies reported as yet on the effect of the contact line capillary number on the dynamic contact angle and hysteresis behavior on hydrophilic and superhydrophobic surfaces for complex fluids. Most of the studies are limited to the static contact angle measurements and spreading dynamics.[27] However, under flow conditions, the dynamics of the three-phase contact line and the resulting dynamic contact angles are known to be influenced by the molecular level adsorption-desorption phenomenon and the macroscopic viscous dissipation.[28,29] From the literature measurements and the theoretical calculations, it is expected that the dynamic advancing contact angle increases with the increase in the three-phase contact point velocity, whereas the dynamic receding contact angle is expected to decrease with the increasing velocity. Several techniques are used to measure the dynamic contact angles. Forced wetting and de-wetting by syringe-driven flows,[30] plunging a surface into a tank using the Wilhelmy plate method,[26] are the most common techniques. The technique of the embedded needle has been in practice for a long period of time[30] but limited to only lower capillary numbers of study.

In the present study, forced wetting and de-wetting experiments are performed by employing the embedded needle syringe-driven flows on colloidal droplets by varying the pumping rates, and the nature of variations of dynamic contact angles on hydrophilic, near hydrophobic, and superhydrophobic surfaces (SHS) is presented. Complex fluids employing only surfactant solutions, nanocolloidal solutions of only particle, and combined surfactant impregnated nanocolloidal solutions are tested at different capillary numbers to understand the flow physics. The nature of variations of the contact angle hysteresis is also inferred for these fluids on these substrates. An index of energy correlating the contact line energy and the dynamic contact angle is also presented, and the transient variations of the line energy are explored for different complex fluids. Also in order to explore the physics of dynamic wetting, a dynamic flow parameter called spreading factor is defined whose transient variations reveal the dynamic response of droplets to perturbation to the three-phase contact point. The present findings shed light on the fundamental understanding of forced wetting and de-wetting of these fluids on a range of substrates that can effectively be utilized to tune the performance of many engineering devices as dipping of substrates in processing solutions, in coating applications, and in general any fluid-structure interactions.

II. EXPERIMENTAL METHODOLOGIES

A. Materials

The experiments are conceived in such a manner as to segregate and understand the contributing effects of different factors affecting the dynamic contact angle hysteresis, such as the surface topographical texture and wettability, the morphology of the nanoparticles, the pumping rate or the contact line capillary number, the concentration of the particles and surfactants, etc. Three surfaces with wettability ranging from hydrophilic (glass slide rendered uniformly hydrophilic in nature by exposing to argon plasma treatment) to near hydrophobic (aluminium Al 6061 grade) to superhydrophobic (commercial coating ultra ever dry applied on a glass slide) have been selected in the present study to understand the effect of wettability on dynamic contact angle hysteresis and contact line pinning. Deionized (DI) water (Millipore, 1–3 μS/cm), metal oxide nanoparticles Al_2O_3 (~45 nm, Sigma-Aldrich, USA), and carbon-based nanocolloidal systems, viz., multiwalled carbon nanotubes (MWCNTs) (20–40 nm external diameter and aspect ratio ~100, Sisco Research Lab, India) and graphene nanosheets, have been considered in the present investigation. Graphene is prepared *in situ* using the two-step procedure by invoking the modified Hummer's method. The detailed procedure is described in the reported literature.[31] The prepared graphene is characterized using High Resolution Scanning Electron Microscopy (HRSEM) and Raman spectroscopy as illustrated in Fig. 1(b). The characteristic D and G bands are observed at ~1355 cm^{-1} and ~1605 cm^{-1}, respectively, which represent the defects and in-plane stretching in graphene, respectively. The presence of 2D band at ~2800 cm^{-1} confirms the presence of graphene, and the ratio of intensity of 2D to G band was around 0.35–4.5 indicating 3-5 layers of graphene.[32]

The present choice of metal and carbon-based nanoparticles ranges over various morphological structures. Figure 1(a) shows the HRSEM image of Al_2O_3 nanoparticles with a near spherical morphology. Figure 1(b) illustrates the graphene nanoflakes with flake-like morphology. Figure 1(c) illustrates the HRSEM image of MWCNTs with tubular morphology. The structure of the coated superhydrophobic surface is revealed by the HRSEM characterization as illustrated in Fig. 1(d). In the present study, sodium dodecyl sulphate (SDS) (anionic, 99% pure, Sisco Research Labs, India) and cetyltrimethylammonium bromide (CTAB) (cationic, 99.5% pure, Sisco Research Labs, India) have been used as the surfactants.

B. Methodology

The experimental protocols are conceived in a way as to clearly segregate and demarcate the effects of surfactants, nanoparticles, and the combined surfactant and nanoparticles in modulating the dynamic contact angle hysteresis on surfaces of varying wettability and to understand the effect of three-phase contact line velocity in modulating it. The objectives of the experiments are to clearly segregate the

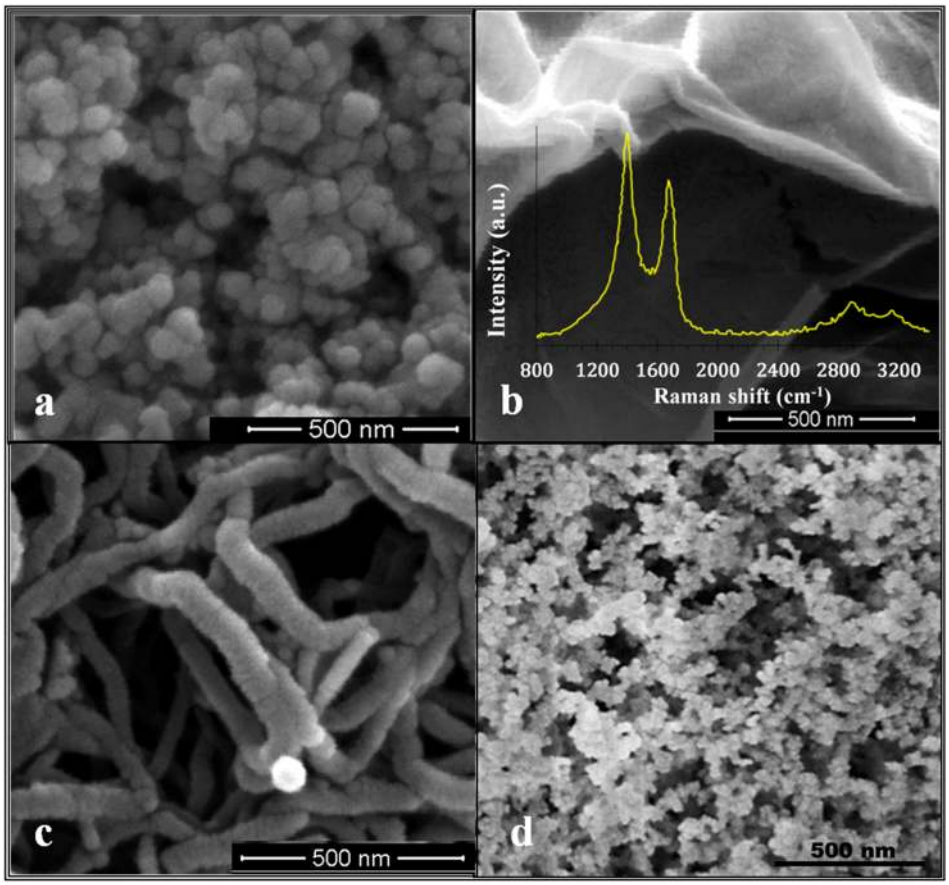

FIG. 1. (a) HRSEM characterization of (~40-50 nm) Al_2O_3 nanoparticles, (b) HRSEM image of graphene nanoflakes showing the flake morphology, (c) HRSEM characterization of MWCNTs, and (d) HRSEM image of the coated superhydrophobic substrate.

contributing effects of nanoparticles and combined nanoparticle and surfactant, the effect of substrate wettability, the effect of capillary number, and the concentrations of the nanoparticle and surfactant in altering the contact angle hysteresis and thereby understanding the pinning effectiveness. The first set of experiments with only a base fluid, i.e., DI water in the present study, forms the datum. The next set of experimental run is designed to elucidate the effect of nanoparticles in which the experiments are conducted with nanocolloidal solutions by dispersing the nanoparticles in the base fluid without the aid of any surfactants. Before conducting the experiments with the combined surfactant and particle effect on wettability, a next set of experiments are planned with only surfactant molecules dispersed in the base fluid (aqueous surfactant solutions). The Critical Micelle Concentration (CMC) values are fixed from our previous reported literature[3] and the surfactant concentration is expressed in a non-dimensionalised form throughout this paper in the form $C_s = C/C_{CMC}$ for each of the surfactants considered in the present study. The experiments are conducted at various concentrations ranging from as low as $C_s = 0.25$ to $C_s = 1.0$ as the post micellar characteristics are not of any interest to the present study. The rheological characterization has been performed for different fluids considered in the present study. The viscosity is almost unaffected by the addition of surfactants for the range of concentrations considered. In the case of nanocolloids of only particles, the viscosities are measured by using a rheometer (Anton Paar) at different particle concentrations. The details have been included in the supplementary material. These colloids are found to be Newtonian in nature. The droplets are generated with an automated syringe pump and the volumes of the sessile droplets generated for all the fluids are near about 3 μl before the start of hysteresis experiments. All the experiments were carried out at 30 ± 2 °C and under relative humidity conditions of 50% ± 5%. All the experiments are conducted three times, and the average value of the contact angle is reported in the manuscript with the uncertainty expressed as two times the variance with a 95% level of confidence. The uncertainties associated with different measurements are also reported in the corresponding figure description.

The present study employed the embedded needle on the sessile drop technique to measure the advancing contact angle (ACA) and receding contact angle (RCA) using a standard goniometer (First Ten Angstroms, USA). The advancing and receding contact angles are measured using the embedded needle measurement method rather than the tilted substrate method. The contact angles are determined from captured video frame images by image processing. The dispensing rate has been programmed so as to vary the pumping in order to capture the effect of capillary number during the pump-in and pump-out stages on modulation of the contact angle hysteresis (CAH). Weighted amounts of particles are dispersed into the accurately measured volume of DI water in preparing the nanoparticle dispersions and are sonicated (Oscar Ultrasonics, India) for requisite amount of time. The experiments are repeated twice and the mean value is reported as the ACA

or RCA with an error corresponding to the deviations in the measurement. The corresponding errors in the measurements have been indicated in figure descriptions.

C. Surface characterization

The glass substrate was rendered uniformly hydrophilic by argon plasma treatment. The aluminium surface is prepared by polishing using diamond paste. The sample is prepared by making use of a wet grinder with a substrate holder so that uniform pressure is applied all over the surface. The average value of the surface roughness obtained is 0.276 ± 0.079 μm (taken over the orthogonal directions at different locations). Detailed AFM characterization of the same sample has been presented in our previous study.[16] The substrates were pre-cleaned by dipping in acetone solution and then DI water and then placing in an oven with vacuum. The same procedure is repeated for cleaning the substrates before conducting the next set of experiments. In order to develop superhydrophobic substrates, the pre-cleaned glass substrates are then coated with the superhydrophobic coating. The coating is a two-step process involving bottom and top coats. The substrate is allowed to dry for 1 h after the application of bottom coat and one day after the application of top coat under ambient atmospheric conditions. The bottom coat acts as a binder for the top coat. After complete drying, a randomly rough micro-metric layer formed on the substrate renders it superhydrophobic as illustrated in the HRSEM image in Fig. 1(d).

III. RESULTS AND DISCUSSIONS

A. Effect of contact line capillary number on dynamic contact angle hysteresis

In order to capture the effect of capillary numbers on the dynamic contact angle, i.e., on the advancing and receding contact angles, the experiments were performed at different pumping rates of pumping out and pumping in through an automated syringe pump at desired volume flow rates of 0.5 μl/s–3 μl/s. Figure S1(a) in the supplementary material illustrates graphically the procedure followed in the present study for the forced wetting and de-wetting and the measurement of ACA and RCA and Fig. S1(b) in the supplementary material illustrates the snapshots of experimental drop shapes at the initial moment, at ACA and at RCA on different substrates (see the supplementary material). Figure 2(a) illustrates the nature of variation of the dynamic contact angle with capillary number on aqueous surfactant droplets at a CTAB surfactant concentration of Cs = 0.25 on the aluminium substrate. The capillary number Ca = μu/σ (where μ represents the viscosity, u represents the velocity of the three-phase contact point of the droplet, and σ corresponds to the effective liquid-vapor surface tension of the complex fluid) is based on the velocity of the movement of the three-phase contact point due to the forced wetting and de-wetting action. The velocity of movement of the three-phase contact line is calculated from the captured image frames. Some of the values of surface tension for different fluids are taken from our previous study.[3] For those fluids, whose surface tension values are not available in the previous literature are measured by the pendant tensiometric method using a standard goniometer. The experimental

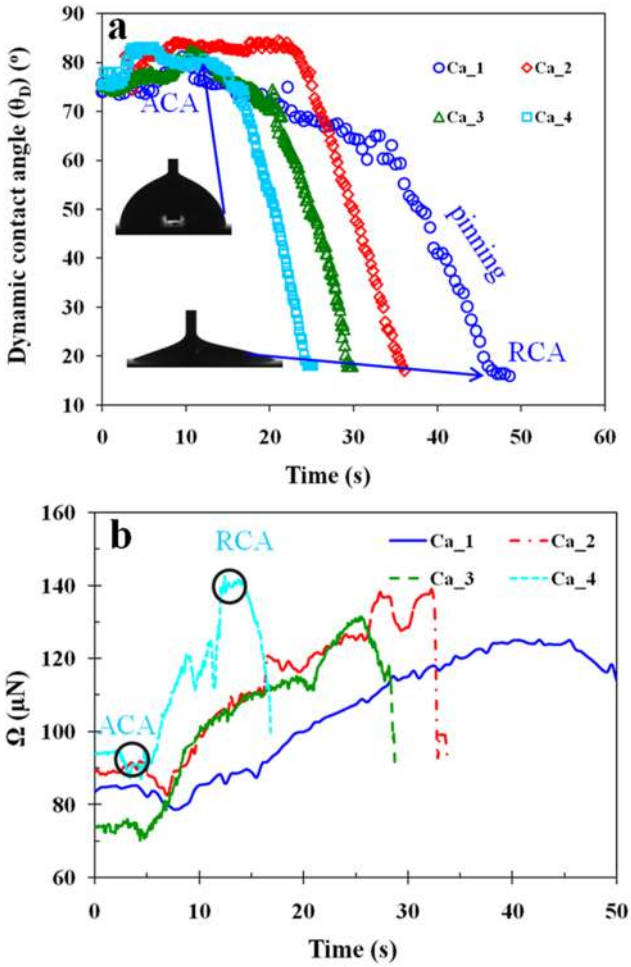

FIG. 2. (a) Variation of dynamic contact angles for CTAB surfactant solution at a concentration of C_s = 0.25 with time at capillary numbers (indicated as Ca_1–Ca_4, Ca_1 = 9.18×10^{-7}; Ca_2 = 1.41×10^{-6}; Ca_3 = 3.81×10^{-6}; Ca_4 = 5.79×10^{-6}) on the aluminium substrate, (b) nature of variation of the line energy (Ω) with time for different capillary numbers mentioned above for the above fluid on the aluminium substrate. The near hydrophobic aluminium substrate showed an uncertainty of ±2.5°-3° with a 95% confidence level for different fluids.

details of surface tension measurement are available in the previous literature.[3] The values of surface tension and viscosity are represented in Tables I–III. More details are available in the supplementary material. It can be observed that there is a slight increment in the value of the ACA but no observable variation in the value of the RCA with the increase in the capillary number. The points of ACA and RCA have been illustrated in the figure. The initial period corresponds to the pump-out mode of operation where the fluid is pumped out at a programmed rate from the syringe pump till the ACA is reached, i.e., the point the three-phase contact line starts to move. Following this, the next phase of the pump-in mode of operation starts. In between the end of the pump-out mode of operation and the beginning of the pump-in mode of operation, there is a transient short period where the droplet spreads by the inertia-driven flow. The pump-in mode of operation is characterized by the pinning of the contact line. After achieving the maximum spreading diameter, the droplet is pinned at the three-phase contact line. As the pump-in mode of operation

TABLE I. Viscosity of nanocolloids at 303 K.

Al_2O_3 (wt. %)	0.1	0.25	0.5	1
Viscosity (mPa s)	0.88	0.952	1.024	1.13
CNT (wt. %)	0.01	0.05	0.1	
Viscosity (mPa s)	0.87	0.93	1.06	
Graphene (wt. %)	0.1	0.25	0.5	
Viscosity (mPa s)	0.886	0.976	1.19	

TABLE II. Surface tension of surfactant solutions.

	Cs = 0.25	Cs = 0.5	Cs = 0.75	Cs = 1
Surface tension of CTAB (mN/m)	62.3	52.1	41.7	39
Surface tension of SDS (mN/m)	57.5	47	40	38

proceeds, the droplet is pinned as illustrated in the figure and the RCA is reached when the three-phase contact point starts to recede.

Figure 3(a) illustrates the nature of variation of the dynamic advancing and receding contact angles at different capillary numbers for water, aqueous surfactant solutions, and nanocolloidal solutions of only particle and combined particle and surfactant nanocolloidal solution on the glass substrate. The advancing contact angles are plotted against the positive capillary number (measured during the pump-out period), while the receding contact angles are plotted against a negative capillary number (measured during the pumping-in period) to differentiate the two regimes. In general, different fluids respond differently to an increase in the three-phase contact line. It can be observed that in the case of water, the advancing contact angle increases with the increase in the capillary number and the receding contact angle decreases for the hydrophilic glass substrate. For water, the changes are significant and the nature of variation is clearly evident from the statical point of view. Although, due to the limitation of the embedded needle syringe-driven flow, the range of the capillary number covered is small, the response of dynamic ACA and RCA is evident for the range of capillary numbers considered. It is clearly evident from Fig. 3(a) that the nature of dynamic wetting of surfactant solutions and nanocolloids (only particle and surfactant-infused nanocolloid) is completely different from that of water. For these fluids, the nature of variation of dynamic ACA and RCA is difficult to judge from the range of capillary number considered. Upon addition of particles, the dynamic ACA shoots up and RCA decreases

TABLE III. Surface tension of nanocolloids.

Surface tension (mN/m) (wt. %)	0.1	0.25	0.5	1
Al_2O_3	71.3	72	72.6	73.1
Al_2O_3 + CTAB (Cs = 0.25)	61	60.7	59.8	59
Al_2O_3 + CTAB (Cs = 0.5)	51	50.3	49.9	49.6
Al_2O_3 + CTAB (Cs = 1.0)	40.3	39.7	39.1	38.5
CNT + SDS (Cs = 0.25)	56.6	56	55.1	54.9
CNT + SDS (Cs = 1.0)	37.5	37.1	37	37.3
Graphene + SDS (Cs = 0.25)	56.3	56	55.6	55.3
Graphene + SDS (Cs = 1.0)	37.6	37	36.9	36.6

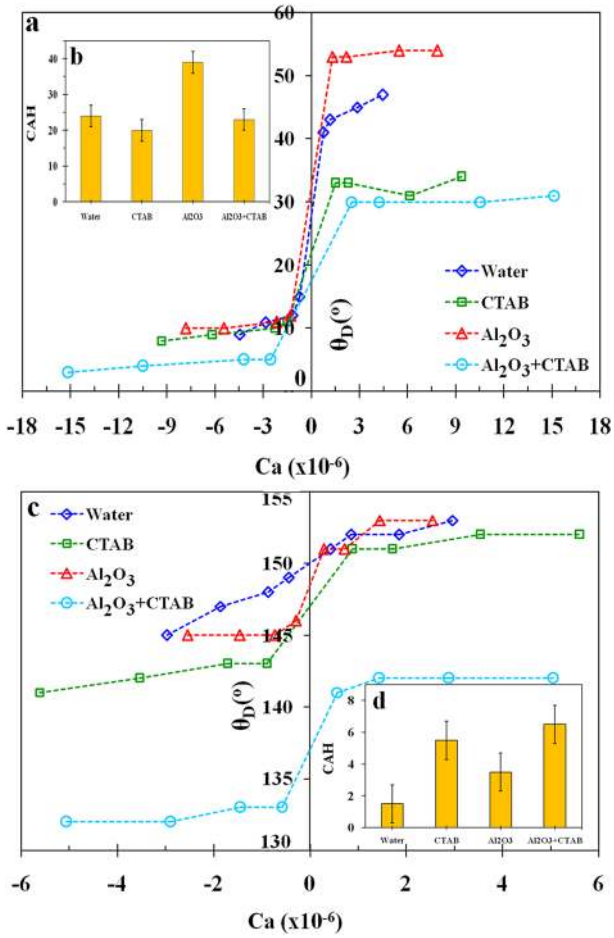

FIG. 3. (a) Variation of the dynamic advancing and receding contact angles with capillary number for water, CTAB solution at a concentration of Cs = 1.0, Al_2O_3 nanocolloidal solution at a particle concentration of 1 wt. % and combined particle and surfactant solution at a concentration of 1 wt. % Al_2O_3, and a CTAB concentration of C_s = 1.0 on the glass substrate, (b) nature of variation of the CAH on the glass substrate for the above fluids, (c) nature of variation of the dynamic contact angles (advancing and receding contact angles) on superhydrophobic substrate (SHS) at different capillary numbers for the above fluids, and (d) CAH variation for the above fluids on SHS. The hydrophilic glass substrate showed an uncertainty of ±2°-2.5°, while the SHS has ±1°-1.5° for different fluids with a 95% confidence level. The lines are only to guide through data points.

compared to water at a given capillary number. However, for surfactant solutions, the ACA decreases and further decreases in the case of surfactant-infused nanocolloids with respect to water. The static ACA and RCA for each data set for different fluids are calculated by extrapolation to zero capillary number using a cubic polynomial fit to the data points at the available capillary numbers.[26] The inferred CAH is shown in Fig. 3(b). Although the mean value of CAH from all the experimental data is bit lower than that of water, statically it is difficult to reach a concrete conclusion. However, the addition of nanoparticles has enhanced the CAH which can be attributed to the local pinning induced due to the layering of particle at the three-phase contact line.[16,18]

The interfacial interactions in complex colloidal systems like combined surfactant and particles are very complex due to the number of interfaces involved and their complex nature of interaction. As the surfactants are added to

the complex nanocolloidal solutions, some of the surfactant molecules interact with the nanoparticles and get adsorbed on the nanoparticle surfaces. The interfacial tension exhibited by the complex colloid is also found to be entirely different from that of its constituents due to the complex interactions present.[3] The surfactant-infused nanocolloids (combined surfactant and nanoparticle nanocolloid) are reported to exhibit an interesting surface tensional behavior. The surface tension of the combined surfactant and nanoparticle nanocolloidal system was found to be lower than that of the surface tension of only surfactant solution at a given concentration of the surfactant.[3] Once the particles are added to the fluid with surfactant molecules, some portion of the total surfactant molecules tries to adsorb at the solid-liquid interface of the particle and base fluid and this depends on the nature of the particle and base fluid. Another fraction of molecules will try to adsorb at the base fluid-air interface. A spherical cap of surfactant molecules adsorbed to the particle will help us to stabilize the suspension. The presence of a foreign nanoparticle in the aqueous surfactant solution modifies the localized adsorption characteristics because of the creation of one more interfacial layer between numerous nanoparticle surfaces and the base fluid which constitute preferential adsorption sites. In the previous studies,[3,16] the authors have observed an enhanced effect of surfactants on interfacial properties in the case of combined surfactants and particle colloidal systems. This was attributed to the particle-driven adsorption to the interface which populated the interface and enhanced the surfactant concentration at the interface. This increases initially with particle concentration at a given surfactant concentration and thereafter it saturates.[3] A similar observation has been reported by Maestro *et al.*,[33] where the concept of the particle as carriers has been discussed. The energetics of particle adsorption desorption are $\sim k_B T$[34] and hence are in dynamic equilibrium between the interface and bulk. Hence the nanoparticle capped with surfactants is driven to the interface as the energetics are less and due to the inherent tendency of the surfactant hydrocarbon chain to go to the vapour interface. It is evident that the addition of surfactants to the nanocolloidal dispersion has lowered the CAH. This can be attributed to the enhanced surfactant effect in surfactant-infused nanocolloidal solutions. The combined particle and surfactant nanocolloid showed a mean value of CAH in between that of only surfactants and only particles.

The adsorption rate to the solid liquid interface and to the liquid vapour interface determines the extent of modulation of the interfacial energy. This can change the wetting characteristics. The adsorption rate is a function of the characteristic property of the adsorbate, the substrate, and the basefluid. The adsorbate may exhibit a characteristic of preferential adsorption to both the interfaces (solid-liquid and liquid vapour). In order to obtain a rough estimate of the ratio of independent adsorption to the solid-liquid and liquid-vapour interface, the Lucassen-Reynders equation is employed for different fluids at different concentrations. The Lucassen-Reynders theory may be expressed as[35,36]

$$\frac{d(\gamma_{lv}\cos\theta)}{d\gamma_{lv}} = \frac{\Gamma_{sv} - \Gamma_{sl}}{\Gamma_{lv}} \approx \frac{-\Gamma_{sl}}{\Gamma_{lv}}, \tag{1}$$

where Γ_{sv}, Γ_{sl}, and Γ_{lv} are the surface excess at the solid vapour interface, solid liquid interface, and liquid-vapour interface, respectively, as described. It is assumed that the adsorption to the solid-vapour interface is zero and hence the ratio of surface excess of solid-liquid with respect to liquid-vapour can be directly evaluated. From the slope of the plot of $d(\gamma_{lv}\cos\theta)$ against $d\gamma_{lv}$, we can directly evaluate the ratio of surface excess. The values of surface tension of different fluids and contact angles are taken from the previous studies.[3,16] With the contact angle information, the ratio of surface excess is evaluated at different surfactants and particle concentrations for all the cases. For CTAB, surfactant solutions on the glass substrate were evaluated and the ratio of Γ_{sl}/Γ_{lv} is found to be 0.659. Hence the glass-surfactant solution interface adsorption is about 65.9% of that of the liquid-air interface. This evaluation is done on the surfactant-infused particle and surfactant case also. The respective values for different cases are indicated in Table S4 in the supplementary material.

When the same case of surfactant is evaluated at different particle concentrations, the ratio gets modified. As indicated in the table, the ratio increases from 0.659 for the pure surfactant case to 0.698 at a small particle concentration of 0.1 wt. %. Upon further increasing the particle concentration to 2.5 wt. % with CTAB surfactant, the ratio again increases to 0.757. This estimate gives a rough picture of population of the adsorbate during static case. However during the pump-in action and during the pump-out action, this will be altered since it is a dynamic system. The above ratio is in accordance with results presented in Fig. 3(a). Here we can observe a similar response for both CTAB solution and CTAB-infused nanocolloid on the glass substrate. This is evident from the ratio of surface excess also as both are in a similar range.

The dynamic wetting characteristics exhibited on superhydrophobic surfaces are found to be different from that observed on hydrophilic surfaces. The literature is scarce about the static wetting characteristics of nanocolloidal drops and combined surfactant impregnated nanocolloidal drops on superhydrophobic substrates and to the best of the authors' knowledge, there is no literature on how it varies with the particle and surfactant concentrations. In the present study, the dynamic wetting characteristics of these complex fluids are dealt with and not the static wetting characteristics. For water, ACA increases with capillary number on superhydrophobic surfaces and the RCA reduces with the increase in capillary number. It is interesting to note that the variation of the dynamic contact angle is significant even for a small range of capillary number considered. Although the complex fluids are also found to behave in a similar manner, the changes are not pronounced for the range of capillary number considered. There is a considerable dip in ACA and RCA from that of only surfactant case for surfactant-infused nanocolloidal solution. Hence it can be inferred that the dynamics of these fluids are different from that of water. The modulation of interfacial energy has a drastic influence on wetting dynamics. The CAH in the case of superhydrophobic substrates for different fluids is different from the trends observed in the case of hydrophilic substrates. Although water exhibits a higher dynamic contact angle hysteresis, the static hysteresis is found to be very low, which is usually a much known characteristic property of

superhydrophobic surfaces as illustrated in Fig. 3(d). Complex fluids of nanocolloidal suspensions and combined surfactant impregnated nanocolloids did not exhibit any observable trend of variation of static contact angle with particle and surfactant concentration on these surfaces. The angle remained more or less the same. Also the dynamic contact angles in the case of complex fluids did not exhibit a remarkable change with capillary number compared to that of water. Due to the surfactant molecules being adsorbed to the solid-vapor interface[37] on superhydrophobic surfaces, the pinning is found to be more and the surfactant solutions are found to exhibit a very high CAH as shown in the figure. The combined surfactant and nanoparticle nanocolloidal solutions exhibited maximum increment in CAH and with a lowest static contact angle.

The nature of variation of the dynamic contact angle with capillary number is found to be similar for surfactant solutions and nanocolloidal solutions at various levels of concentrations of surfactants and particles on hydrophilic substrates as illustrated in Fig. 4. For colloidal solutions, the particle effect is

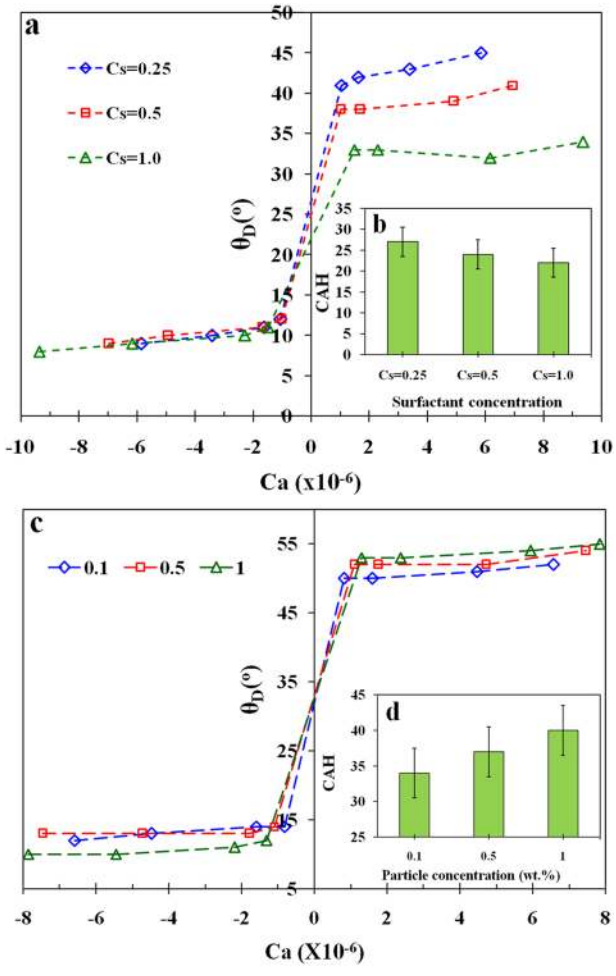

FIG. 4. (a) Dynamic contact angle variation (advancing and receding contact angles) at different CTAB surfactant concentrations for different capillary numbers on the glass substrate, (b) CAH variation with surfactant concentration on the glass substrate, (c) dynamic contact angle variation at different particle concentrations of Al_2O_3 on the glass substrate with respect to capillary number, and (d) CAH variation with particle concentration for the above case. The hydrophilic glass substrate showed an uncertainty of ±2°-2.5° with a 95% confidence level. The lines are only to guide through data points.

to increase the hysteresis as the particles are more effective in altering the pinning dynamics of the three-phase contact line.[16,36] The modulation of the solid-liquid interfacial energy and the effective pinning at the three-phase contact point effectively modulate the hysteresis behavior in complex fluids. The adsorption desorption of surfactants and nanoparticles is a diffusion-driven process and will not influence in dynamic wetting and de-wetting operations, as the time scales of the different processes are different.[39] The interfacial adsorption of surfactants and particles is diffusion driven and it is a slow process. It is observed to be a function of nature of adsorbate, viz., the surfactant and nanoparticles from our previous study on transient surface tension response of these fluids.[3] The time scale adsorption varies for the surfactant solutions, nanocolloids of only particles, and nanocolloids of combined surfactants and nanoparticles. However, we did not notice a considerable difference in adsorption time with concentration for the surfactant alone, particle alone, and combined surfactant and particle case for the range of concentration studied. The adsorption time is around 30-40 s for colloidal solutions of only particle, around 100 s for surfactant solutions, and 90-100 s for combined surfactant and particle nanocolloids. The pump in process or the dynamic wetting study has been performed after the initial spreading of the droplet is completed for the whole study. The spreading experiment has been conducted initially on these substrates by the authors.[20] The present experimental study is a dynamic study where the droplet interface is dynamically perturbed by either the pump-in or pump-out action. However the perturbation frequency is very low as the time scale of the pump-out and pump-in action varies between 20 s and 60 s. This will change the surface area available for the adsorption. Hence the active sites for adsorption are dynamically varying. Also during pump-in, more adsorbates are pumped in and the internal flow inside the droplet also is very dynamic. However, as the CAH is a local phenomenon near the three-phase contact line, the adsorption during dynamic perturbation will not affect the results. The CAH and the dynamic wetting behavior exhibited by different complex fluids depend greatly on the initial or equilibrium surface tension of these complex fluids.[3,16] However, the initial surface tension of these fluids dictates the wetting behavior and the pinning at the three-phase contact point and hence influencing the CAH.[16] As reported in the earlier literature,[3] the surface tension of the nanocolloids will increase with increase in the particle concentration, and hence the contact line pinning at the three-phase contact point which results in the increase in the CAH as illustrated in Fig. 4(d).

B. Modeling the three-phase contact point line energy

Applying energy balance and equating the total work change to the energy change,[40]

$$\delta w = \gamma_{lv} dA_{lv} + \gamma_{sl} dA_{sl} + \gamma_{sv} dA_{sv} + \Delta P dV - \Omega(t) dl, \qquad (2)$$

where l is the circumference of the drop-substrate contact area, Ω is the energy per unit length associated with an extra increment in the circumferential length dl. γ_{lv}, γ_{sv}, and γ_{sl} are the interfacial energies at the liquid-vapor interface, solid-vapor interface, and solid-liquid interface, dA represent the differential change in area, and dV is the change in volume due

to change in the Laplace pressure which is induced indirectly through the pump-in and pump-out action,

$$\delta w = \gamma_{lv} dA_{lv} + (\gamma_{sl} - \gamma_{sv}) dA_{sl} + \Delta P dV - \Omega(t) dl. \quad (3)$$

When $\delta w = 0$ and on dividing both sides of Eq. (2) by dA_{sl}, the following expression can be obtained:

$$\gamma_{lv} \frac{dA_{lv}}{dA_{sl}} + \gamma_{sl} - \gamma_{sv} + \frac{\Delta P dV}{dA_{sl}} - \Omega(t) \frac{dl}{dA_{sl}} = 0. \quad (4)$$

It has been shown in the literature[40] that at a particular point of time for a given constant volume, it can be expressed from the geometrical relationship that

$$\frac{dl}{dA_{sl}} = \left(\frac{\pi}{3} \frac{(2 - 3\cos\theta + \cos^3\theta)}{V \sin^3\theta} \right)^{1/3}, \quad (5)$$

and also from the geometrical relationship for a droplet on a substrate, it can be derived that

$$\frac{dA_{lv}}{dA_{sl}} = \cos\theta_D, \quad (6)$$

where θ_D is the dynamic contact angle at a particular instant of time. Using Eqs. (5) and (6) in (4), the following expression is obtained:

$$\gamma_{lv} \cos\theta_D + \gamma_{sl} - \gamma_{sv} + \frac{\Delta P dV}{dA_{sl}} - \Omega(t) \times \left(\frac{\pi}{3} \frac{(2 - 3\cos\theta + \cos^3\theta)}{V(t) \sin^3\theta} \right)^{1/3} = 0. \quad (7)$$

In order to quantify the line energy, that is, how much energy is needed to be invested to obtain θ_D, the line energy can be expressed as a function of θ_D, volume V(t), and the interfacial energies. Also using classical Young's contact angle relationship and rearranging, the line energy can be expressed as

$$\Omega(t) = (\gamma_{lv} \cos\theta_0) V(t)^{1/3} \left(\frac{1}{\cos\theta_0} \cos\theta_D - 1 + \frac{\Delta P dV}{dA_{sl} \gamma_{lv} \cos\theta_0} \right) \times \left(\frac{3}{\pi} \frac{\sin^3\theta_D}{(2 - 3\cos\theta_D + \cos^3\theta_D)} \right)^{1/3}, \quad (8)$$

where θ_0 is the Young equilibrium contact angle.

This can be further approximated as (see the supplementary material)

$$\Omega(t) = (\gamma_{lv} \cos\theta_0) V(t)^{1/3} \left(\frac{1}{\cos\theta_0} \cos\theta_D - 1 + \frac{\sin^2\theta_D}{\cos\theta_0 \cos\theta_D} \right) \times \left(\frac{3}{\pi} \frac{\sin^3\theta_D}{(2 - 3\cos\theta_D + \cos^3\theta_D)} \right)^{1/3}, \quad (9)$$

where $\Omega(t)$ represents the instantaneous line energy and θ_D represents the dynamic contact angle variation. The equilibrium contact angle θ_0 is fixed for a given fluid droplet on a particular substrate. The equilibrium contact angles for the present study are taken from the previous literature on static contact angles[16] and the transient volume is measured by post processing the captured images.

Figure 2(b) illustrates the nature of variation of the line energy for the CTAB solution at a concentration of Cs = 0.25 for different capillary numbers. The line energy slightly increases or almost remains constant during the pump-out stage till the ACA is reached and the peak value of the line energy corresponds to the ACA. Once the droplet crosses the ACA, during the pinned mode, energy continuously increases. This period corresponds to the pump-in mode of action, and as it progresses, the line energy increases and reaches the maximum value. The maximum corresponds to the RCA where the three-phase contact line starts to retract inwards. After the maximum peak in the line energy, the energy drops as the contact line starts to retract. The natures of variation in the line energy at all levels of pumping rates are similar. Nevertheless the most interesting observation is that the maximum line energy points corresponding to the ACA and RCA points vary with different levels of pumping. So irrespective of the pumping rate, the maxima of the line energy curves are almost the same in magnitude. Also it is noteworthy that the effective pinning constant τ_p can be defined as $\tau_p = \frac{t_p}{t_t}$, where t_p is the effective pinning time and t_t is the total time. The effective pinning constant is found to be the same in all the cases of capillary number and its value is around ~0.68 in all the cases.

Figure 5(a) illustrates the nature of variation of the dynamic contact angle in the case of surfactant solutions at different concentrations. The observations are at a pumping rate of 0.5 μl/s on the aluminium substrate. It can be observed that irrespective of the surfactant concentration, the time to reach RCA is almost the same for a given pumping rate. The nature of variation is similar at all concentrations of surfactant. For the above particular case, the nature of variation of the line energy is illustrated in Fig. 5(b). Line energy data for water are also illustrated, which forms the reference datum. However the capillary number varies as indicated in the figure description. The magnitude of variation in line energy in the case of water is very low compared to that of the surfactant solutions. Upon adding the surfactants to water, the line energy increases as it is observed in Fig. 5(b). At a concentration of Cs = 0.25, the line energy for retraction is very large compared to that of the water. However, on increasing the surfactant concentration, the magnitude of the line energy decreases and approaches that of the water case. It can be attributed to the fact that as the surfactants are added to the systems, it adsorbs to the interface and modulates the interfacial energies[16] and hence the flow-ability nature. These interfacial energy modulation will ultimately result in altering the pinning effectiveness as we can observe distinct energy levels for different surfactant concentrations.

In order to track the effect of particle concentration on the nature of variation of the line energy, the values are deducted from the experimental observations of dynamic contact angle variation on the aluminium surface at different particle concentrations at a pumping rate of 0.5 μl/s. The capillary number variation is indicated in the figure description. There is an observable change in the magnitude of Ω of the colloidal solutions at different particle concentrations. However, the curves show the similar nature of variation as illustrated in Fig. 5(c). However, it is interesting to note that the value has considerably increased from that of only water case. As the particle concentration increases, the Ω also increases. This can be attributed to the enhanced pinning at the three-phase contact point by the colloidal solutions. As the particle concentration increases, the pinning also increases[16]

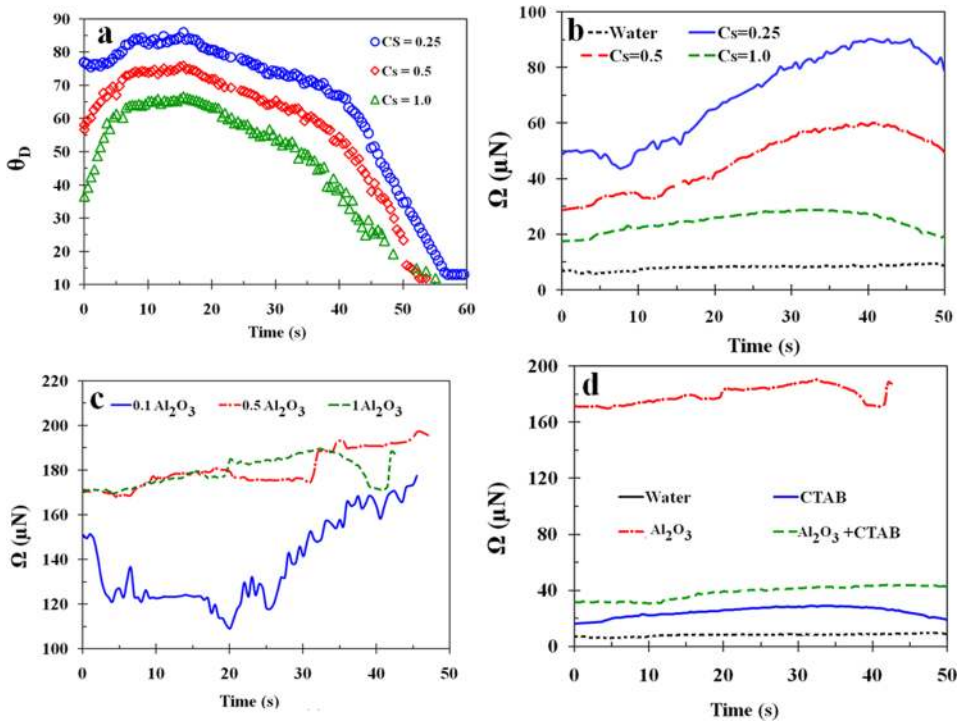

FIG. 5. (a) Dynamic contact angle variation with time at a pumping rate of 0.5 μl/s for CTAB surfactant solution at different surfactant concentrations on the aluminium substrate, (b) nature of variation of line energy (Ω) with time for CTAB surfactant solutions at various concentrations of surfactants on the aluminium substrate (capillary number varies as follows : Ca_C_s_0.25 = 9.33×10^{-7}; Ca_C_s_0.5 = 1.2×10^{-6}; Ca_C_s_1.0 = 1.41×10^{-6}; Ca_water = 7.41×10^{-7}), (c) line energy variation with time in the case of nanocolloids of only particle at different particle concentrations on the aluminium substrate (capillary number varies as follows: Ca_0.1 = 8.11×10^{-7}; Ca_0.5 = 1.11×10^{-6}; Ca_1.0 = 1.33×10^{-6}), and (d) line energy variation with time for different solutions D I water (Ca = 7.41×10^{-7}), CTAB at a concentration of C_s = 1.0 (Ca = 1.37×10^{-6}), 1 wt. % Al_2O_3 (Ca = 1.33×10^{-6}) and combined surfactant and nanoparticle colloidal systems at a concentration of C_s = 1.0 and 1 wt. % Al_2O_3 (Ca = 1.79×10^{-6}) on the aluminium substrate at a pumping rate of 0.5 μl/s.

due to augmented particle interactivity with the substrate at the three-phase contact line and the particle layering at the three-phase contact point. This results in increment in the numerical value of the Ω. However, the change in energy from 0.5 wt. % to 1 wt. % is not appreciable as it seems to have shown a saturated behavior because of the saturation in the pinning effectiveness and retarded transport of particle to the three-phase contact line. Although it is difficult to compare the variation of line energy at a constant capillary number, we can draw a general conclusion about the nature of line energy variation with particle and surfactant concentration at a capillary number as the variations in capillary numbers are not huge. Similar observation has been reported in the earlier literature[16] where a saturation in the contact angle hysteresis behavior after this concentration in a similar substrate. Figure 5(d) illustrates the comparison of energy variation in the case of different complex fluids. Only particle nanocolloidal solutions exhibit the maximum line energy, and the addition of surfactants decreases the pinning effectiveness and brings down the energy levels.

In order to understand the nature of variation of the dynamic contact angle in case combined surfactant and nanoparticle colloidal systems, the study has been extended to combined colloids on different substrates with different pumping rates. The nature of variation of the dynamic contact angles on different substrates was similar in nature to that observed in the case of nanocolloids of only particles and surfactant solutions at all pumping rates. Figure 6(a) illustrates the effect of CTAB surfactant concentration for a given particle concentration of 1 wt. % Al_2O_3 for the combined particle and surfactant solutions. It can be observed that as in the earlier cases, the nature of variation of line energy remains almost the same for all the fluids tested. The line energy increases with the surfactant concentration for a given particle concentration up to some concentration and then decreases. It can be attributed to the fact that as the surfactant concentration increases, more particles are transported to the interface[3] and to the three-phase contact line which results in more pinned mode and the receding energetics are affected because of this. But after a certain concentration, the steric repulsion hiders the interfacial transport and hence results in decrease in pinning effectiveness and bringing the energy down. However, for a given particle concentration, upon increasing the particle concentration, the line energetics vary as illustrated in Fig. 6(b). However, it is to be noted that the addition of surfactants to the nanocolloidal solutions of particles resulted in a reduction in the magnitude of these energetics. Hence it can be elucidated that a velocity and concentration of complex fluid-dependent line energy exists on the forced retraction mode of a sessile droplet on a substrate. Also it is to be noted that the addition of surfactants (with the change in surfactant concentration for a given particle concentration) is capable of altering the line energy drastically as compared to the vice versa case. This reaffirms the fact that in a combined colloidal system, the surfactant effect is dominating as reported earlier.[16]

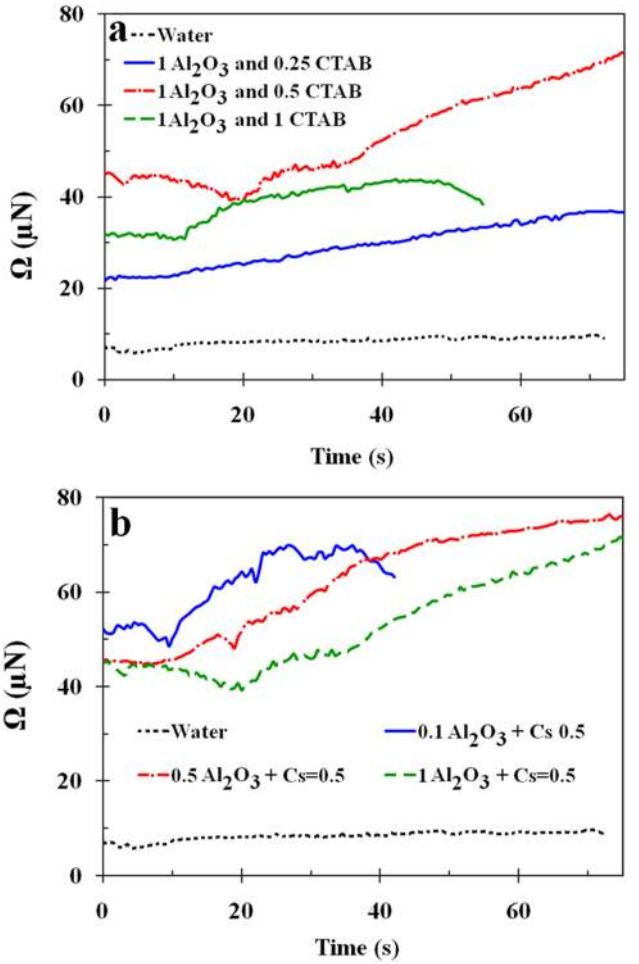

FIG. 6. Illustration of nature of variation of line energy (Ω) with time for combined surfactant and nanoparticle colloidal systems on the aluminium substrate at a pumping rate of 0.5 μl/s (a) at a given Al_2O_3 particle concentration of 1 wt. % and at different surfactant concentrations (Ca_1Al_2O_3_Cs_0.25 = 1.31×10^{-6}; Ca_1Al_2O_3_Cs_0.5 = 1.60×10^{-6}; Ca_1Al_2O_3_Cs_1.0 = 2.05×10^{-6}) and (b) showing the effect of particle concentration at a given CTAB surfactant concentration of C_s = 0.5 (Ca_C_s0.5_0.1Al_2O_3 = 1.23×10^{-6}; Ca_ C_s0.5_0.5Al_2O_3 = 1.57×10^{-6}; Ca_ C_s0.5_1.0Al_2O_3 = 1.83×10^{-6}).

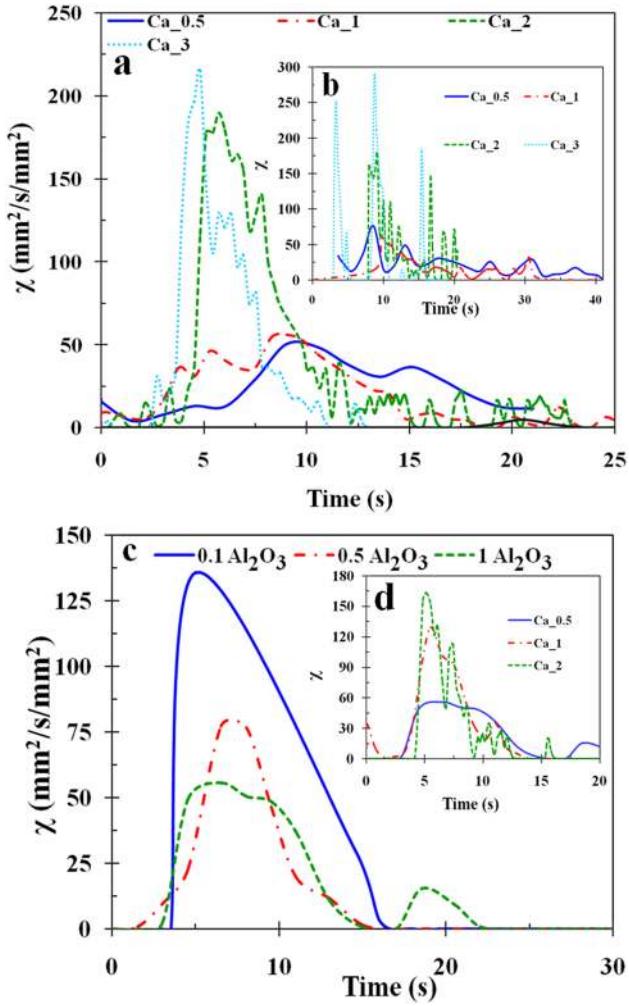

FIG. 7. Flow curve illustrating the nature of variation of spreading factor χ with time for (a) CTAB aqueous surfactant solutions at a concentration of C_s = 0.25 at different pumping rates illustrating the effect of velocity of three-phase contact line capillary numbers (Ca_0.5 = 9.18×10^{-7}; Ca_1 = 1.42×10^{-6}; Ca_2 = 3.83×10^{-6}; Ca_3 = 5.81×10^{-6}), (b) CTAB aqueous surfactant solution at a concentration of C_s = 1.0 at different contact line capillary numbers (Ca_0.5 = 1.46×10^{-6}; Ca_1 = 2.27×10^{-6}; Ca_2 = 6.16×10^{-6}; Ca_3 = 9.35×10^{-6}), (c) Al_2O_3 nanocolloids at different concentrations at a pumping rate of 0.5 μl/s (Ca_0.1 = 9.1×10^{-7}; Ca_0.5 = 1.06×10^{-6}; Ca_1 = 1.31×10^{-6}), and (d) Al_2O_3 nanocolloid (at 1 wt. %) at different capillary numbers illustrating the effect of velocity of three-phase contact line movement (Ca_0.5 = 1.36×10^{-6}; Ca_1 = 2.21×10^{-6}; Ca_2 = 6.16×10^{-6}).

C. Dynamic flow curve

In depth, physics of the dynamic wetting behavior at different capillary numbers corresponding to the movement of the three-phase contact point can be elucidated from the flow curve as illustrated in Fig. 7. The observations of the transient flow physics will reveal the dynamic wetting and the interfacial fluid-structure interaction which resembles many practical situations encountered in real engineering problems. The rate of change of the wetting area of the liquid droplet gives an indication of the transient fluid-structure interaction. However, the rate of change of droplet surface area is an indication of the extent of spreading and the flow-ability of the droplet. It is a function of the resulting contact angle, the interfacial tensions, and the effective pinning at the three-phase contact point. So the physics of the dynamic wetting can be captured from the observations of the transients in these parameters. The present study defines a parameter called the spreading factor $\chi(t)$ which can be defined as $\chi(t) = \frac{\dot{A}_w}{A_s}$ where $\dot{A}_w$ is the rate of change of wetting area at a given instant of time and A_s is the dynamic surface area of the droplet at that particular instant of time. The spreading factor is a coupling term combining the cause and the effect as described earlier in the case of forced wetting and de-wetting. The primary objective of the present study is to understand the dynamic advancing and receding contact angle and thereby dynamic contact angle hysteresis by pump-out and pump-in at different rates to achieve different velocities of three-phase contact line movement, and the secondary objective is to understand the dynamic spreading characteristics while spreading after the attainment of ACA and receding after RCA during forced wetting and de-wetting conditions. The dynamic flow curve helps us to understand the flow physics such as: the area under the curve is an indication

of extent of spreading, the peaks indicate the attainment of ACA, the magnitude of peak is an indication of extent of sudden expansion after attainment of ACA and it increases with pumping rate. Hence these features can be understood from one figure with relevant time scale. The numerical magnitude is only taken in the present analysis in the case of both the forced wetting period and de-wetting period. Figure 7(a) illustrates the flow curve exemplifying the nature of variation of spreading factor ($\chi(t)$) with time in the case of forced wetting for aqueous surfactant solutions at a CTAB concentration of $C_s = 0.25$ at different capillary numbers.

The peak in the curve represents the attainment of ACA and the movement of the three-phase contact point. As the three-phase contact point starts suddenly moving, there is a sudden increment in $\dot{A}_w$ which results in the maxima of the flow curve. The jump in the curve decays out slowly in the case of surfactant solution at almost similar capillary number regimes. It may be due to the fact that the spreading tendency of aqueous surfactant solutions is more. Due to the interfacial adsorption by the surfactant molecules, the interfacial energies are altered and this results in spreading. Till achieving a capillary number of 1.51×10^{-6}, i.e., corresponding to pumping rate 1 μl/s, the magnitude of the peak remains the same; however, the area under the curve increases with the increase in the capillary number due to the enhanced spreading at higher pumping rates. Upon further increase in the capillary number, the peak shifts toward left indicating an achievement of ACA at a faster pace due to enhancement in the pumping action. Also the magnitude of the peak increase is high compared to that at lower capillary numbers. This indicates a sudden increment in the wetting area with respect to the surface area. Figure 7(b) illustrates a similar flow curve at an enhanced critical surfactant concentration of Cs = 1 indicating the effect of contact line capillary numbers. As the contact line capillary number increases, the magnitude of the peak also increases. The flow curve is similar to that observed at Cs = 0.25.

The nature of the forced wetting and de-wetting in the case of particle laden drops will be different from that of the aqueous surfactant solutions. In the case of colloidal drops of only particle, the particle transport to the three-phase contact point drastically alters the effective movement of the three-phase contact point. It has been observed earlier that the particles are effective in pinning the three-phase contact point.[16] However further understanding the dynamics of the three-phase contact point movement and effective dynamic pinning and de-pinning while undergoing forced wetting and de-wetting at different forcing rates can be captured from the dynamic spreading factor curve. The effect of particle concentration in modulating the three-phase contact point movement and effect on the transient spreading factor is illustrated in Figs. 7(c) and 7(d). As the particle concentration increases, the magnitude of the peak of the flow curve decreases indicating an enhanced pinning at a higher particle concentration and higher viscous dissipation and greater resistance to the movement of the three-phase contact point. The viscous dissipation tends to slow down the movement of the three-phase contact movement. However, the particle layering at the three-phase contact point and the structural component of disjoining pressure results in an enhanced spreading of the nanofluids.[26] This fact is evident from the comparison of the magnitude of the peaks in the spreading factor curves of the surfactant solutions and that of the nanocolloidal solutions. The magnitude of the peak of the spreading factor is higher in the case of nanocolloidal solutions compared to that of the surfactant solutions. Hence the present observations prove the earlier observations and also cement the fact that the observations are valid in the case of forced wetting and de-wetting also which are encountered mostly in engineering devices.

The effect of surfactant concentration on the flow curve at a given pumping rate is discussed in the supplementary material. Also, it is interesting to observe the physics of dynamics of flow behavior in the case of combined surfactant and nanoparticle nanocolloid for the forced wetting and de-wetting case at different pumping rates and at different combinations of concentrations of particles and surfactants. The details are available in the supplementary material.

D. Effect of particle morphology

The present study involves particles of three entirely different morphologies such as spherical Al_2O_3, tubular CNTs, and flake-like graphene nanoparticles. Figure 8(a) characterizes the effect of morphology on the glass substrate when the droplet of the nanocolloidal solution is subjected to forced wetting and de-wetting under a pumping rate of 0.5 μl/s. All the nanocolloidal solutions are prepared at a particle concentration of 0.1 wt. % and at a surfactant concentration of Cs = 0.25 as the nanocolloidal solution of CNTs and graphene is not stable without the presence of surfactants. As seen from Fig. 8(a), the advancing contact angle increases with the capillary number. However, although the receding contact angle decreases with increasing capillary number, the changes are not appreciable as observed in the case of advancing contact angle. The contact angle hysteresis is plotted against the average capillary number of all the three fluids at different pumping rates as illustrated in Fig. 8(b). The average capillary number is calculated as the simple average of capillary numbers obtained at a given pumping rate. The dynamic contact angle hysteresis was calculated from the difference between the dynamic ACA and the dynamic RCA. It is to be noted that the results presented in the present study correspond to the variations at lower capillary numbers.

The contact angle hysteresis is a local phenomenon and depends in general on the surface heterogeneities, roughness, liquid adsorption, or desorption, etc.[7] However, there is no concrete consensus and full understanding of the hysteresis phenomenon on smooth and chemically homogeneous surfaces, as yet.[7] Our study is on nanofluids and also on dynamic contact angle hysteresis which adds to the complexity of the problem. It has been observed from the previous studies that the particle layering occurs at the three-phase contact line for nanocolloidal droplets[16–18] which can alter the disjoining pressure due to the addition of the structural component of disjoining pressure. Hence the aggregation of particle (or surfactant-infused particle) near the three-phase contact line results in localized pinning[38] and alteration of the surface morphology. This in fact affects the contact angle hysteresis. The structural component of disjoining pressure is a function of the

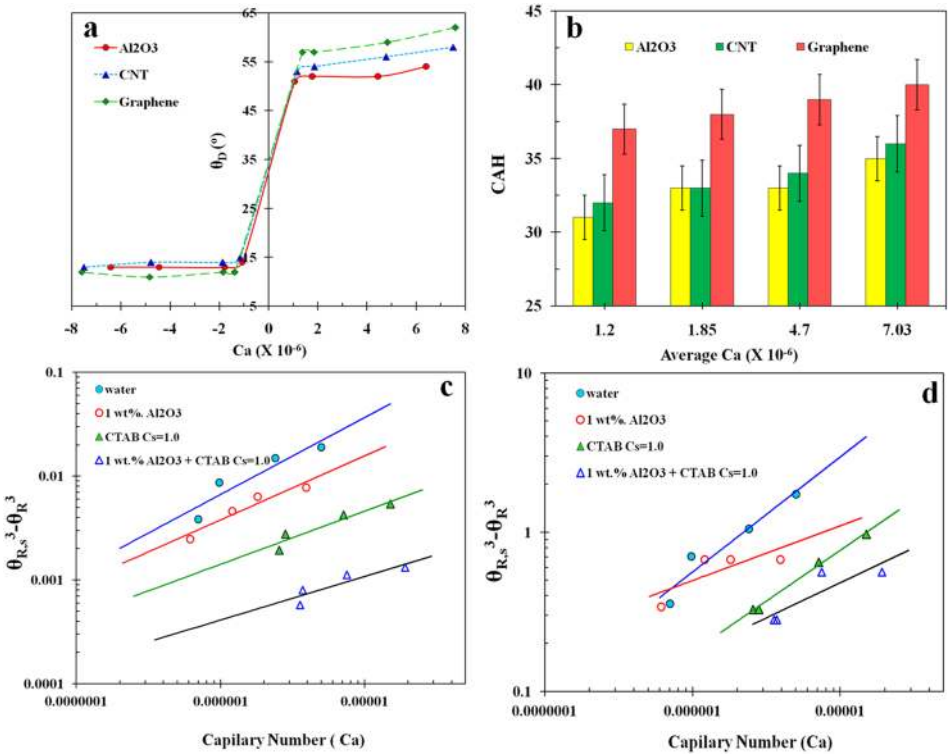

FIG. 8. (a) Effect of particle morphology illustrating the nature of variation of the dynamic contact angle with the pumping rate for 0.1 wt. % Al_2O_3 and 0.25 CMC CTAB nanocolloid, 0.1 wt. % MWCNT and 0.25 CMC SDS nanocolloid, 0.1 wt. % graphene and 0.25 CMC SDS nanocolloids on the glass substrate. (b) Variation of contact angle hysteresis for the above case, (c) plot of the difference in cube of the static receding contact angle and cube of the dynamic receding contact angle as a function of capillary number for water, nanocolloidal solutions of 1 wt. % Al_2O_3, surfactant solutions at a concentration of C_s = 1.0, and combined nanocolloidal solution of 1 wt. % Al_2O_3 and C_s = 1 CTAB solution on the glass substrate, and (d) plot of the difference in cube of the static receding contact angle and cube of the dynamic receding contact angle as a function of capillary number for above fluids on the superhydrophobic surface.

size and morphology of the particle.[41] The particle layering at the three-phase contact point and hence the local pinning and the disjoining pressure (of which mainly the structural component of disjoining pressure as the other components are negligible[20]) greatly influence and modify the ACA and RCA which alter the static as well as dynamic contact angle hysteresis.

The pump in process or the dynamic wetting study has been performed after the initial spreading of the droplet is completed. The spreading experiment has been conducted initially on these substrates by the authors.[20] In this sessile droplet, the capillary flow inside the droplet carries the particles to the three-phase contact line and hence results in pinning. However during the pump-in and pump-out process, the flow is altered and hence this can again locally modify the particle distribution near the contact line. This ultimately results in modification of local pinning, modification of local (near the contact line) surface topography, and disjoining pressure. However all these are functions of particle morphology and hence result in modification of contact angle hysteresis. Graphene with flake-like morphology shows the maximum dynamic contact angle hysteresis as a function of capillary number. Followed by graphene, tubular CNTs have the next highest dynamic hysteresis. However, the magnitude difference between the dynamic contact angle hysteresis of CNTs and Al_2O_3 is not much evident. It can be elucidated that under the similar conditions, the particles with different morphologies exhibit different dynamic contact angle hysteresis. However, in a previous report by present authors,[16] it has been elucidated that the effective interactions are responsible for deciding the effective CAH. The present study also observes a similar result as although CNTs with tubular morphology are expected to have higher CAH, the CAH magnitude in the case of Al_2O_3-based nanocolloid and CNT-based nanocolloid is similar in magnitude. The dynamic CAH is found to increase in all the colloidal solutions irrespective of the morphology and the rate of increment being a function of the particle and surface interaction characteristics. The effective viscous stress is apparent in the variation of the CAH.[26] Though the material properties differ for the nanoparticles selected, this study gives a general picture on the effect of morphology. More detailed study with the same material properties but having different morphologies can bring out deeper physics of the problem.

E. Correlation with the capillary number

In order to mathematically model the trends of receding contact angles and to compare the hydrodynamic mode as expressed in Eq. (8), the slip length is invoked. The slip length is a direct manifestation of deviation from the no-slip mode at the wall to the Navier slip condition during receding of the thin film of liquid along the interface. Knowledge of the magnitude of slip length enables deducing the role and interactivity of the surfactant/nanoparticles at the fluid–substrate and their influence vis-à-vis the nature of motion of the complex fluid contact line. To this end, the Cox-Voinov-Tanner law is invoked and the slip length is scaled from the information of the receding contact angle of different fluids. In this approach, the difference between the cubes of the static and dynamic receding contact angles is expressed as a function of the contact line capillary number and a power law formulation is achieved. The index of the contact line capillary number for a given fluid on a given substrate indicates the magnitude of the deviatory behavior of the dynamic receding angle with respect to the static receding angle and thereby provides information regarding the propensity of the fluid to wet or de-wet the particular surface. The data for different fluids with respect

to hydrophilic glass and superhydrophobic surfaces are fit to the capillary number with the closest match index in Figs. 8(c) and 8(d).

The static contact angle of each data set for different fluids is calculated by extrapolation to zero capillary number using a cubic polynomial fit to the data points at the available capillary numbers as described earlier. Considering the flow close to the three-phase contact line, the no slip-boundary condition will result in infinite viscous stress in the fluid. This results in stress singularity, which makes the solution of the Navier-Stokes equation impossible for a moving contact line problem. Voinov developed a hydrodynamic relation[42] between the contact line speed and contact angle of the droplet by allowing a finite slip for very small capillary number regimes. Tanner developed a similar scaling model for completely wetting droplets[43] which is referred as the Cox-Voinov-Tanner law. For partially wetting fluids, they derived an exact solution which can be expressed as[44]

$$\theta_D{}^3 = \theta_S{}^3 \pm (9\mu U/\gamma)\ln(L/b), \tag{10}$$

where L is the characteristic length scale of the outer region of the flow, b is the slip length, θ_S is the static contact angle. The outer length scale is usually expressed as $L = \alpha\sqrt{\gamma/\rho g}$, where $\sqrt{\gamma/\rho g}$ is the capillary length. The previous study reports that constant α is a function of flow geometry, boundary conditions, and capillary numbers of the flow. An estimate of the slip length in the present study as per the formulation for α as suggested by Eggers[45] was found to be 3.871 μm in the case of water on hydrophilic substrates. The change in slip length due to the addition of particles is found to be negligible compared to that of water as the addition of particles has brought about only negligible change in interfacial characteristics.[3] However, the addition of surfactant resulted in the decrease of slip length to 2.5 μm.

As seen from Fig. 8(c), the receding contact angle data for all the fluids considered on the glass substrate are found to scale like $\theta_{R,S}{}^3 - \theta_R{}^3 \; \alpha \; Ca$ as predicted by the hydrodynamic Cox-Voinov-Tanner scaling law as shown by the fit superimposed on the data points. $\theta_{R,S}$ and θ_R indicate the static receding contact angle and the dynamic receding contact angle. It is to be noted that the advancing contact angle behavior is also similar to that of receding contact angles and found to be fairly proportional to the capillary number. So, irrespective of the nature of the complexity of the fluids, the fluids are found to obey the hydrodynamic theory predicted on the hydrophilic substrate at a very low capillary number. Similar observations are recorded by Kim *et al.*[26] by using the Wilhelmy plate method for pure water receding along the hydrophobic polytetrafluoroethylene (PTFE) substrate. Hence regardless of the nature of the substrate, it obeys the scaling law as per the hydrodynamic equation. However, in contrast to the earlier observations, the behavior of advancing (although not shown in the figure) and receding contact angles is found to be more complex than that observed in the case of hydrophilic substrates. The data points seem to be little more scattered than that in the case of the hydrophilic substrate fit by the Cox-Voinov-Tanner scaling law. However as our experiments are confined to very small capillary number regimes, it appears to follow the scaling.

IV. CONCLUSION

The present study comprehensively explores the dynamic wetting characteristics of complex colloidal solutions under forced wetting and de-wetting on a range of substrates from hydrophilic smooth glass to near hydrophobic aluminium to superhydrophobic substrates. The extent of variation of the dynamic ACA, RCA, and the contact angle hysteresis depends on the nature of substrates, and the fluid and is a strong function of capillary number. The morphology of the particle is found to play a major role in deciding the variations of the dynamic contact angles and strongly influences the dynamic contact angle hysteresis. Similar to polymeric solution,[20] a velocity-dependent force is observed. It is found that a velocity and concentration of complex fluid-dependent line energy exists on the forced retraction mode of a sessile droplet on a substrate from the transient line energy analysis. Segregated analysis brought a clear picture of forced wetting dynamics of surfactant impregnated nanocolloids. The dynamic flow characteristics are found to be different for different fluids and the physics of dynamic wetting has been captured using a spreading factor for each case. The dynamic contact angles measured on smooth hydrophilic substrates were found to fairly obey the Cox-Voinov-Tanner law with capillary number even for the complex fluids as in normal fluids.[16] The degree of dependency varies for different fluids; however, in the case of superhydrophobic surfaces, the data showed a weaker dependence thereby further highlighting the strong influence of the surface wettability. Further in depth, slip mechanisms in the case of complex fluids can further shed light on the mechanism at nanoscale.

SUPPLEMENTARY MATERIAL

See supplementary material for:

1. Experimental illustration and snapshots.
2. Theoretical calculation of different geometrical aspects of a sessile droplet.
3. Dynamic flow curve.
4. Rheological and surface tension characteristics of nanocolloids.
5. Ratio of surface excess.

ACKNOWLEDGMENTS

P.D. would like to thank IIT Ropar for the financial support towards the present research (vide ISIRD grant IITRPR/Research/193). A.R.H. would also like to thank Ministry of Human Resources, Govt. Of India for the doctoral scholarship.

[1] S. K. Das, S. U. Choi, and H. E. Patel, "Heat transfer in nanofluids—A review," Heat Transfer Eng. **27**, 3–19 (2006).
[2] A. R. Harikrishnan, S. K. Das, P. K. Agnihotri, and P. Dhar, "Particle and surfactant interactions effected polar and dispersive components of interfacial energy in nanocolloids," J. Appl. Phys. **122**, 054301 (2017).
[3] A. R. Harikrishnan, P. Dhar, P. K. Agnihotri, S. Gedupudi, and S. K. Das, "Effects of interplay of nanoparticles, surfactants and base fluid on the surface tension of nanocolloids," Eur. Phys. J. E **40**, 53 (2017).
[4] P. G. De Gennes, "Wetting: Statics and dynamics," Rev. Mod. Phys. **57**, 827 (1985).
[5] A. Marmur, "Soft contact: Measurement and interpretation of contact angles," Soft Matter **2**, 12–17 (2006).

[6]E. M. Blokhuis and B. Widom, "Wetting," Curr. Opin. Colloid Interface Sci. **1**, 424–429 (1996).
[7]H. B. Eral and J. M. Oh, "Contact angle hysteresis: A review of fundamentals and applications," Colloid Polym. Sci. **291**, 247–260 (2013).
[8]M. A. Rodríguez-Valverde, F. J. M. Ruiz-Cabello, P. M. Gea-Jódar, H. Kamusewitz, and M. A. Cabrerizo-Vílchez, "A new model to estimate the Young contact angle from contact angle hysteresis measurements," Colloids Surf., A **365**, 21–27 (2010).
[9]E. Chibowski, "On some relations between advancing, receding and Young's contact angles," Adv. Colloid Interface Sci. **133**, 51–59 (2007).
[10]E. Chibowski, A. Ontiveros-Ortega, and R. Perea-Carpio, "On the interpretation of contact angle hysteresis," J. Adhes. Sci. Technol. **16**, 1367–1404 (2002).
[11]G. Lu, X. D. Wang, and Y. Y. Duan, "A critical review of dynamic wetting by complex fluids: From Newtonian fluids to non-Newtonian fluids and nanofluids," Adv. Colloid Interface Sci. **236**, 43–62 (2016).
[12]C. Huh and L. E. Scriven, "Hydrodynamic model of steady movement of a solid/liquid/fluid contact line," J. Colloid Interface Sci. **35**, 85–101 (1971).
[13]T. D. Blake, "The physics of moving wetting lines," J. Colloid Interface Sci. **299**, 1–13 (2006).
[14]T. D. Blake and J. M. Haynes, "Kinetics of liquid liquid displacement," J. Colloid Interface Sci. **30**, 421–423 (1969).
[15]P. Petrov and I. Petrov, "A combined molecular-hydrodynamic approach to wetting kinetics," Langmuir **8**, 1762–1767 (1992).
[16]A. R. Harikrishnan, P. Dhar, P. K. Agnihotri, S. Gedupudi, and S. K. Das, "Wettability of complex fluids and surfactant capped nanoparticle-induced quasi-universal wetting behaviour," J. Phys. Chem. B **121**, 6081 (2017).
[17]S. Vafaei, T. Borca-Tasciuc, M. Z. Podowski, A. Purkayastha, G. Ramanath, and P. M. Ajayan, "Effect of nanoparticles on sessile droplet contact angle," Nanotechnology **17**, 2523 (2006).
[18]S. Vafaei, D. Wen, and T. Borca-Tasciuc, "Nanofluid surface wettability through asymptotic contact angle," Langmuir **27**, 2211–2218 (2011).
[19]R. G. Chaudhuri and S. Paria, "The wettability of PTFE and glass surfaces by nanofluids," J. Colloid Interface Sci. **434**, 141–151 (2014).
[20]A. R. Harikrishnan, P. Dhar, S. Gedupudi, and S. K. Das, "Effect of interaction of nanoparticles and surfactants on the spreading dynamics of sessile droplets," Langmuir **33**, 12180–12192 (2017).
[21]D. T. Wasan and A. D. Nikolov, "Spreading of nanofluids on solids," Nature **423**, 156 (2003).
[22]D. L. Hu, B. Chan, and J. W. Bush, "The hydrodynamics of water strider locomotion," Nature **424**, 663 (2003).
[23]N. J. Shirtcliffe, G. McHale, M. I. Newton, C. C. Perry, and F. B. Pyatt, "Plastron properties of a superhydrophobic surface," Appl. Phys. Lett. **89**, 104106 (2006).
[24]Y. Zheng, X. Gao, and L. Jiang, "Directional adhesion of superhydrophobic butterfly wings," Soft Matter **3**, 178–182 (2007).
[25]M. Nosonovsky and B. Bhushan, "Superhydrophobic surfaces and emerging applications: Non-adhesion, energy, green engineering," Curr. Opin. Colloid Interface Sci. **14**, 270–280 (2009).
[26]J. H. Kim, H. P. Kavehpour, and J. P. Rothstein, "Dynamic contact angle measurements on superhydrophobic surfaces," Phys. Fluids **27**, 032107 (2015).
[27]G. McHale, N. J. Shirtcliffe, and M. I. Newton, "Contact-angle hysteresis on super-hydrophobic surfaces," Langmuir **20**, 10146–10149 (2004).
[28]P. G. De Gennes, F. Brochard-Wyart, and D. Quéré, *Capillarity and Wetting Phenomena: Drops, Bubbles, Pearls, Waves* (Springer Science & Business Media, 2013).
[29]J. C. Berg, *Role of Acid-Base Interactions in Wetting and Related Phenomena* (Marcel Dekker, New York, 1993), Vol. 75.
[30]M. I. Smith and J. S. Sharp, "Origin of contact line forces during the retraction of dilute polymer solution drops," Langmuir **30**, 5455–5459 (2014).
[31]P. Dhar, M. H. D. Ansari, S. S. Gupta, V. M. Siva, T. Pradeep, A. Pattamatta, and S. K. Das, "Percolation network dynamicity and sheet dynamics governed viscous behavior of polydispersed graphene nanosheet suspensions," J. Nanopart. Res. **15**, 2095 (2013).
[32]N. Kurra, V. S. Bhadram, C. Narayana, and G. U. Kulkarni, "Few layer graphene to graphitic films: Infrared photoconductive versus bolometric response," Nanoscale **5**, 381–389 (2013).
[33]A. Maestro, E. Guzmán, E. Santini, F. Ravera, L. Liggieri, F. Ortega, and R. G. Rubio, "Wettability of silica nanoparticle–surfactant nanocomposite interfacial layers," Soft Matter **8**, 837–843 (2012).
[34]C. Zeng, H. Bissig, and A. D. Dinsmore, "Particles on droplets: From fundamental physics to novel materials," Solid State Commun. **139**, 547–556 (2006).
[35]E. H. Lucassen-Reynders, "Contact angles and adsorption on solids1, 2," J. Phys. Chem. **67**, 969–972 (1963).
[36]M. D. Doganci, B. U. Sesli, and H. Y. Erbil, "Diffusion-controlled evaporation of sodium dodecyl sulfate solution drops placed on a hydrophobic substrate," J. Colloid Interface Sci. **362**, 524–531 (2011).
[37]A. J. B. Milne, J. A. W. Elliott, and A. Amirfazli, "Contact angles of surfactant solutions on heterogeneous surfaces," Phys. Chem. Chem. Phys. **17**, 5574–5585 (2015).
[38]L. Espín and S. Kumar, "Forced spreading of films and droplets of colloidal suspensions," J. Fluid Mech. **742**, 495–519 (2014).
[39]D. Fell, G. Auernhammer, E. Bonaccurso, C. Liu, R. Sokuler, and H. J. Butt, "Influence of surfactant concentration and background salt on forced dynamic wetting and dewetting," Langmuir **27**, 2112–2117 (2011).
[40]R. Tadmor, "Line energy and the relation between advancing, receding, and Young contact angles," Langmuir **20**, 7659–7664 (2004).
[41]K. Kondiparty, A. Nikolov, S. Wu, and D. Wasan, "Wetting and spreading of nanofluids on solid surfaces driven by the structural disjoining pressure: Statics analysis and experiments," Langmuir **27**, 3324–3335 (2011).
[42]O. V. Voinov, "Hydrodynamics of wetting," Fluid Dyn. **11**, 714–721 (1976).
[43]L. H. Tanner, "The spreading of silicone oil drops on horizontal surfaces," J. Phys. D: Appl. Phys. **12**, 1473 (1979).
[44]J. Eggers, "Contact line motion for partially wetting fluids," Phys. Rev. E **72**, 061605 (2005).
[45]J. Eggers, "Existence of receding and advancing contact lines," Phys. Fluids **17**, 082106 (2005).